Medical Informatics

ISSN: 0307-7640 (Print) (Online) Journal homepage: http://www.tandfonline.com/loi/imif18

Evaluation of a CCD-based facial measurement system

A. T. Deacon, A. G. Anthony, S. N. Bhatia & J.-P. Muller

To cite this article: A. T. Deacon, A. G. Anthony, S. N. Bhatia & J.-P. Muller (1991) Evaluation of a CCD-based facial measurement system, Medical Informatics, 16:2, 213-228, DOI: 10.3109/14639239109012128

To link to this article: http://dx.doi.org/10.3109/14639239109012128

Published online: 12 Jul 2009.

MED. INFORM. (1991), VOL. 16, NO. 2, 213–228

Evaluation of a CCD-based facial measurement system

A. T. DEACON†, A. G. ANTHONY†, S. N. BHATIA‡ and J.-P. MULLER§

† Thorn EMI Research, Hayes, Middlesex UB3 1HH, UK
‡ King's College School of Medicine and Dentistry, London SE5 8RX, UK
§ Department of Photogrammetry and Surveying, University College London, WC1E 6BT, UK

(*Received 12 November 1990*)

Abstract. This paper describes the configuration and evaluation of a CCD-based biostereometric system at the Department of Orthodontics, Kings College Dental Hospital, London. The system has been designed to allow rapid and accurate measurement of facial soft-tissue shape with a minimum of traditional photogrammetric training. This has been achieved by automatic camera calibration and stereo matching, performed on a Sun Microsystem 3/160 workstation. In summary, the characteristics of the system are: (*a*) non-contact three-dimensional (3D) measurement of soft-tissue; (*b*) de-skilled, requiring little or no photogrammetric training; (*c*) rapid data acquisition, combined with slower off-line processing; (*d*) processing of resulting 3D surface information to yield cross-sections; (*e*) surface measurement accurate to within 0·5 mm. Accuracy assessment was performed using a manual electromechanical non-contact measurement device with precision exceeding the requirement of the biostereometric system.

Keywords: Biostereometrics; Soft-tissue morphology; Three dimensions; Photogrammetry.

1. Introduction

Biostereometrics can be defined as the spatial and spatiotemporal analysis of biological form utilizing the principles of analytical geometry. The widespread use of biostereometrics has been restricted by the time and cost factors involved in the acquisition of accurate, comprehensive three-dimensional measurements of human soft tissue. Conventional anthropometric methods, based on the use of calipers, offer uncomplicated and practical two-dimensional assessment but are inadequate for the task of surface characterization. Optical non-contact techniques, such as light stripe scanning systems [1], Moiré fringing, laser scanning systems [2] and stereo-photogrammetry offer potential solutions. Our aim has been to evaluate automated stereophotogrammetry.

Close-range stereophotogrammetry, in which two or more images taken from different viewpoints are analysed to yield spatial information, has been used in biometric studies since the early 1930s [3] and has been successfully applied to facial measurement [4]. Traditional stereophotogrammetry requires the use of film emulsions and expensive pre-calibrated *metric* cameras. The last decade saw the development of low-cost charge coupled device (CCD) cameras that utilize geometrically stable arrays of light-sensitive silicon. Such cameras offer the advantage of image capture in a format suitable for digital input to computer systems and subsequent automatic analysis.

The mathematical foundations of stereophotogrammetry can, with some adaptation, be applied to the new imaging technology to allow the determination of spatial

0307-7640/91 $3·00

information. For a small number of points on an object the location and measurement can be performed at or near the rate at which video information is received from the camera [5]. This is not possible at measurement densities necessary to describe the human face faithfully.

If the cost and performance criteria can be satisfied, measurement of body form has a multitude of applications. Notable examples include:

(1) *Facial.* Monitoring of swelling [6], anthropometric studies of genetic disorders [7], surgery planning [8], surgery assessment [9], growth studies [10], objective abnormality description.
(2) *Spinal deformity.* Quantified description and assessment.
(3) *Lung function.* Chest shape monitoring in breathing analysis [11].
(4) *Seating design.* Avoidance of pressure points for wheelchair users.
(5) *Body and limb volume.* Space travel studies [12], obesity studies.

The automated close-range photogrammetry described in this paper is based on collaborative research, conducted as part of Alvey† project MMI-137 *Real-time 2·5D Vision Systems*, into the development and use of this technology for measurement of industrial objects at Thorn EMI Central Research Laboratories and University College London. It was found particularly suited to measuring 'sculptured' surfaces such as those encountered in the car and aerospace industries. The optical characteristics of human flesh and the limited categories of surface likely to be encountered make biostereometrics an important non-industrial application of the technology. The Orthodontic Department at King's has for some time been interested in the biometric procedures for studying facial morphology and growth. An interactive on-line computer system for diagnosis, treatment planning and prediction of postoperative soft-tissue profile (based on two-dimensional radiography) has been developed [13]. Recent areas of research have included the automatic stereo matching of digitized 35 mm negatives [14], measurement of facial contours from photographs and electromechanical non-contact measurement [15].

2. System configuration

The automated biostereometric system is shown diagrammatically in figure 1.

The photographic facial measurement studies at King's have used an array of eight 35 mm SLR film cameras mounted on a semicircular mounting bracket, 2 m in diameter, for image acquisition. A standard X-ray cephalostat, mounted at a height of 2 m, is used to position the patient during image capture. A small hydraulic platform is used to raise the patient to the cephalostat where earplugs ensure reduced degrees of rotational freedom. These are useful for gross realignment of the patient for comparative analysis in the future.

Image acquisition in the automated close-range photogrammetry system is by means of a pair of COHU 4710 frame transfer CCD cameras with an array size of 699 × 580 pixel, fitted with 35 mm CCTV lenses. These cameras are connected to a 68010-based framestore capable of capturing stereo pairs simultaneously.

In order to make spatial measurements from the stereo images the system must know where the cameras are positioned in space, and their orientation relative to a common frame of reference. This reference coordinate system is provided by a calibration object, originally constructed for the industrial studies at Thorn EMI,

† The UK Alvey programme was part funded by the Department of Trade and Industry, the Science and Engineering Council and the Ministry of Defence.

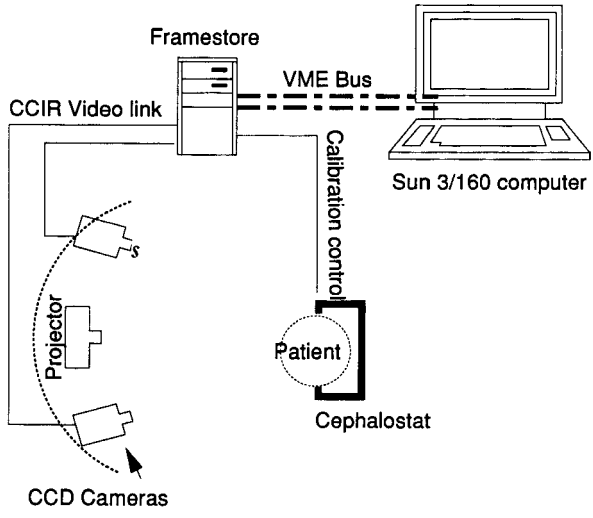

Figure 1. Biostereometric systems configuration.

placed in the field of view of the cameras before a series of measurements is made. The camera model and method of determining the parameters are described in the next section.

The calibration object (which is critical to the overall measurement performance of the system), consists of three flat plates, fabricated from a stable cast aluminium alloy, connected at right angles to form a corner-shaped object. Each plane contains a 6×6 grid of holes spaced at 50 mm, holes drilled to a precision of $\pm 0{\cdot}02$ mm by a numerically controlled drilling machine. The hole positions and squareness of the planes were checked on a coordinate measuring machine at the quality assurance department of Thorn EMI Electronics Radar Division, producing accurate positional data for each hole which can be used in place of the nominal positions if necessary. Flat-top light-emitting diodes (LEDs) were inserted into these holes that act as *active* calibration targets providing excellent signal-to-noise ratios in the calibration images captured from the camera video signal, avoiding the use of complex target-detection algorithms.

This high-precision calibration target has been used to allow rigorous validation of the camera calibration algorithm and stereo matching software. It is envisaged that future biostereometric camera calibration will be based on a simpler target field incorporated into the cephalostat.

A Sun Microsystem 3/160 workstation is used to process the camera calibration images, process patient images to yield spatial data and store all associated records.

3. Camera calibration

Camera calibration is the process of determining a set of parameters which define the two-dimensional (2D) image position of a given 3D object point. These parameters fall into the categories of *interior* and *exterior*.

The interior orientation (figure 2) defines the position of the imaging plane with respect to the optical centre of the lens (known as the principal distance or effective focal length, F) and the position at which the optical axis of the lens intersects the image plane (known as the principal point, or point of symmetry). In addition it is possible to include the distortion properties of the imaging lens.

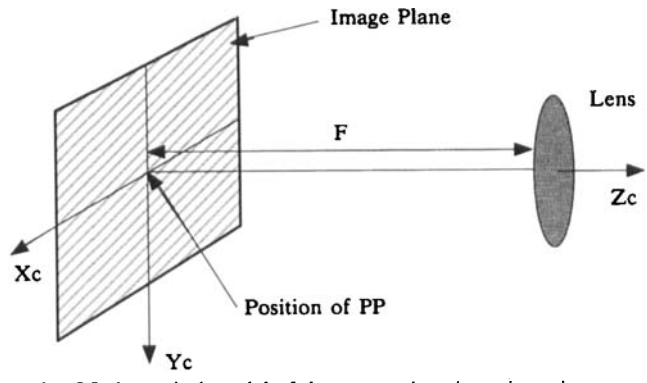

Figure 2. Mathematical model of the camera interior orientation parameters.

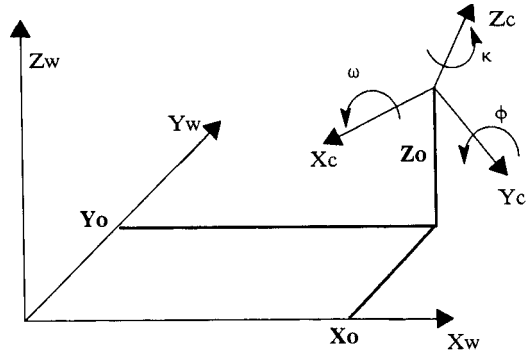

Figure 3. Mathematical model of the position and orientation of lens centre and optical axis.

The external orientation defines the position and orientation of the camera system with respect to some external reference frame. The position of the camera is given by the 3D coordinates of the lens optical centre and its orientation is given by the Euler rotation angles omega, phi and kappa taken about the X, Y and Z axes of the world system (figure 3).

Metric cameras are designed specifically for photogrammetric purposes and are equipped with fiducial marks that define a precalibrated interior orientation. All other professional and amateur cameras are considered non-metric. These have the advantage of being more generally available, and are usually more flexible in their focusing range. However, the lenses are designed for high resolution at the expense of distortion. In addition these cameras lack fiducial marks and consequently have an unknown interior orientation. CCD cameras, designed primarily for television and surveillance work, fall into the non-metric category.

The problems of calibrating metric and non-metric cameras are well known in photogrammetry. More recently, as the emphasis on real-time systems has increased, attention has been given to the use and calibration of CCD cameras and the new problems that they entail [16].

Close-range camera calibration generally utilizes images of a field of targets of known 3D coordinates. The mathematical method employed in this biostereometric system was first proposed by Tsai [17]. It is a two-stage technique based on the observation that, irrespective of radial lens distortion, the vector from the principal point to a particular image point is parallel to the vector drawn from the extended

optical axis to the corresponding object space point. The radial lens constraint allows the unknown parameters to be solved for in two steps (hence 'two-stage'), each of which involves the solution of a set of linear equations. Because both steps are linear the technique does not require approximate knowledge of the values of the unknowns, which is always difficult to obtain with any non-metric camera.

Tsai's model also allows us to consider the scale factor which defines the relationship between the number of samples along a line on the CCD array and the number of samples along a line in the framestore memory.

The principal point (PP), defined as the position where the optical axis of the lens intersects the imaging array (figure 2), cannot be included as an unknown in this model. Instead it has been determined by a single measurement at the start of the study using a direct optical method similar in principle to auto-collimation [18].

The quality of camera calibration is usually assessed in terms of the residual error of the image coordinates produced by the transformation of the nominal 3D calibration points using the calculated parameters. For this system the mean image plane residuals are approximately 1·5 pixel.

4. Operational details

One significant advantage of the use of electronic image acquisition over photographic film is the ease of interactive image assessment. In this system monitors provide real-time feedback of the video signals from the cameras, allowing any focusing or positional adjustments to be made. Any camera adjustments must be made before the system is calibrated; patient position can of course be adjusted at any stage. This feature can be an advantage in positional registration of a patient with previously acquired image data.

The calibration object, shown in figure 4, is positioned in the cephalostat. The host computer then instructs the framestore to capture images of the reference LEDs under its control and transfer these via the VME bus to the disk storage. A subset of LEDs from a given plane are used to determine the origin of the reference coordinate

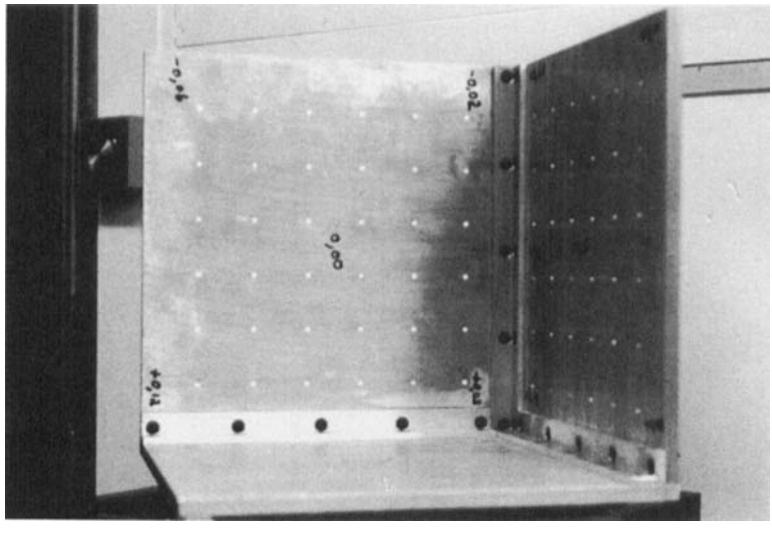

Figure 4. Calibration field constructed of aluminium alloy.

system, and the orientation of the plane axis, as shown in figure 5. This information is used in the second image in which all LEDs for the given plane are illuminated. This procedure is repeated for the other two planes.

The end-result of this process is a list of 2D image positions for each LED together with the absolute 3D coordinates on the global reference frame. It is these data that are used to determine the position and orientation of the camera, as explained in the previous section.

Although the numerical processing of the calibration data is performed separately for each camera the calibration images themselves can be acquired by both cameras simultaneously. The image acquisition and processing required for automatic calibration takes less than 60 s, and need only be performed routinely once or twice a day and on each occasion that the cameras are moved or refocused.

The calibration object is then removed and the patient is raised up to the cephalostat on the hydraulic platform. Diffuse lighting does not produce image pairs suitable for automatic stereo matching due to the low pixel intensity variance. An example is seen in figure 11. Instead, the patient's face is illuminated with a random-intensity dot pattern used in the previous industrial studies (figure 6), or the subtle grid pattern (figure 7) that was used in the original photographic-based contour measurement work. The grid pattern has the significant advantage that important anatomical landmarks are still clearly visible [19].

When the operator decides that the position and expression are acceptable, the framestore 'freezes' the image data, which can be subsequently transferred to the host computer for direct display on the high-resolution screen. As the image capture time is 1/25 s, image blur due to patient movement is very rare.

The operator now selects *seed* stereo matches, consisting of the image coordinates of a visible feature in the left image and the image coordinates of the corresponding feature in the right image. These are measured on the workstation screen using a

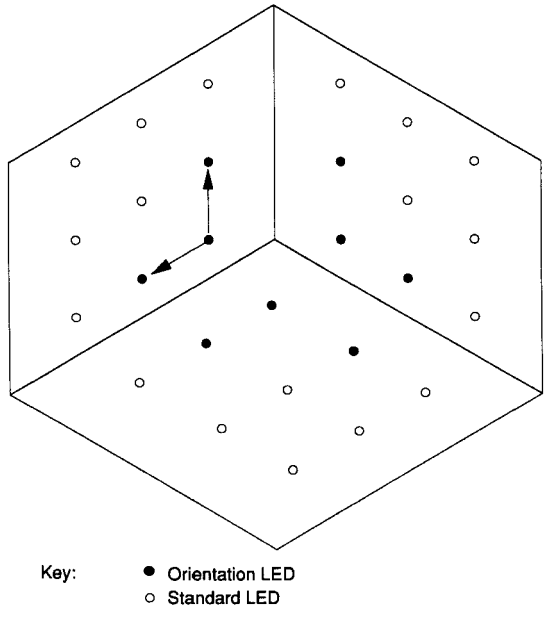

Figure 5. 'Orientation' LEDs mounted in calibration plate.

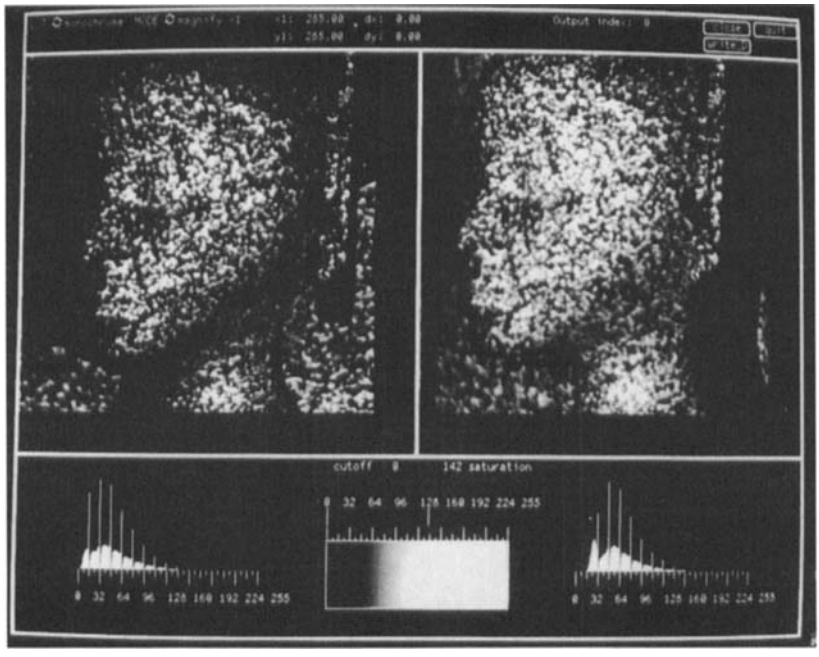

Figure 6. Stereo pair of images displayed on the workstation showing unstructured textured light projection used to assist automatic stereo matcher.

mouse. Each of these seed stereo matches can be used to determine a *disparity* vector linking the image points. The distance between the cameras and the point on the surface is a function of this disparity vector. Five or six disparity values are required to allow the automatic *sheet growing* stereo matching algorithm, developed at University College London [20], to be applied to the images. The algorithm refines each of the operator's estimates using adaptive least-squares correlation [21], yielding an improved disparity value and a quality metric. The 'best' pair of image coordinates is chosen and an additional disparity *estimate* is generated by taking the left image coordinate to be the neighbouring pixel and determining the right image coordinate using the *current* disparity value. The new estimate is then refined producing a new disparity value, the change reflecting the spatial displacement of the points being measured on the surface. Using this technique the algorithm propagates the disparity information over the face, stopping at points in the images where the quality metric indicates that a spatial boundary has been reached.

Stereo matching is the most computationally expensive part of the process; disparity values are calculated at the rate of two per second on the 4 MIPs Sun 3/160. In order to minimize the processing time and yet still measure sufficient stereo disparity values in the images the 'neighbour' of a point in the left image is taken as a being five pixels away. Thus the left image coordinates of the disparity values all lie on a grid of spacing five pixels. A full-face description consists of between 4000 and 6000 data points.

Disparity data are combined with the camera position and orientation data to yield 3D coordinates by means of *analytical space intersection*. This process involves the setting up of virtual projection rays from each camera that pass through the optical centres and the points on the imaging planes defined by the disparity values. In general these rays do not intersect exactly, due to errors in the determination of

Figure 7. Projected grid pattern with 1·5 mm spacing on face. Used in manual contour work and automated stereo matching.

both the disparity data and the camera parameters. Instead the midpoint of vector of closest approach of these rays is taken as the 3D coordinate on the surface. The length of this vector is termed *residual parallax*, and is typically 0·1 mm over a distance of 2 m for this system. Complete processing of all disparity values takes only a few seconds.

Using standard computer graphics and computer-aided design (CAD) techniques the surface data can be rendered and processed to simulate the appearance of the patient as the soft-tissue shape is altered. An example of a rendered model is given in figure 8. In figure 9 the surface data have been interpolated to produce a contour plot, and in figure 10 a wireframe visualization can be seen. In the King's system, software allows cross-sections to be determined through planes defined by points on the original images.

5. Assessment of accuracy

The accuracy assessment of any measurement system is essentially an operation that compares a reference data set with the results obtained from the system under test. In this case the complexity of the surface being measured—reflected in the number of 3D data points required to describe the entire surface faithfully—presents

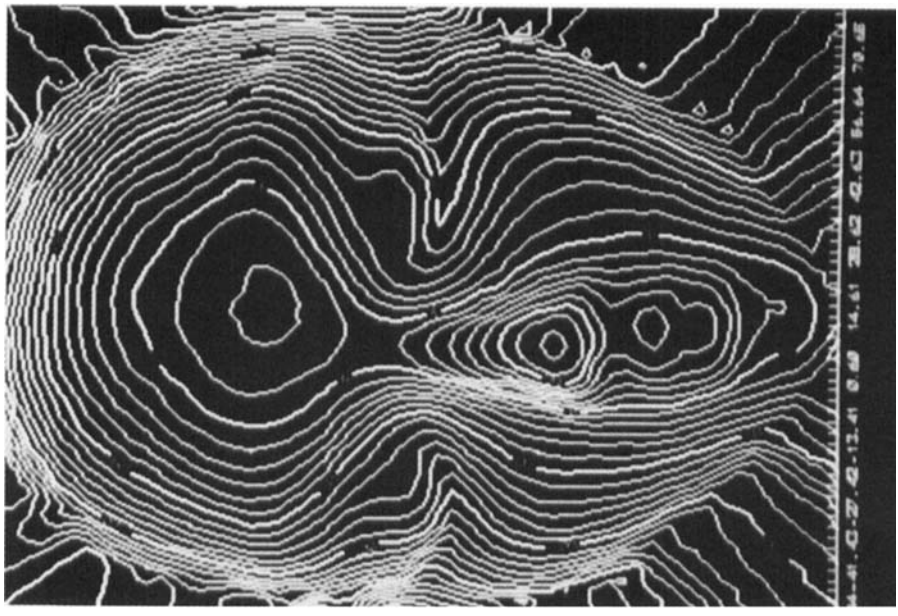

Figure 9. Contour plot of reference model interpolated from 3D data measured by the system.

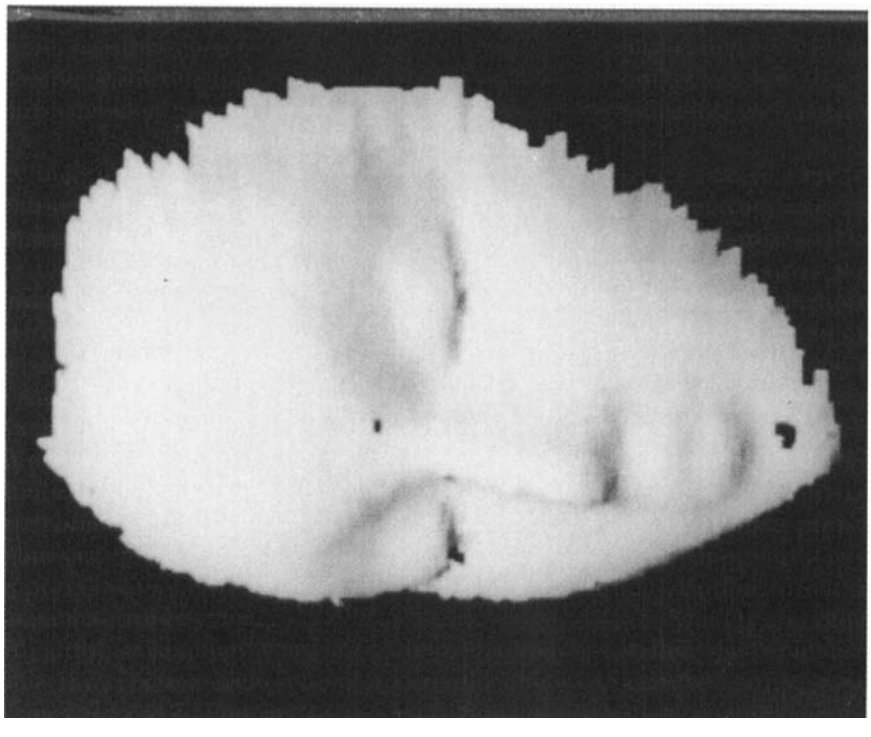

Figure 8. Visualization of reference model 3D surface data using computer graphics and simulated illumination.

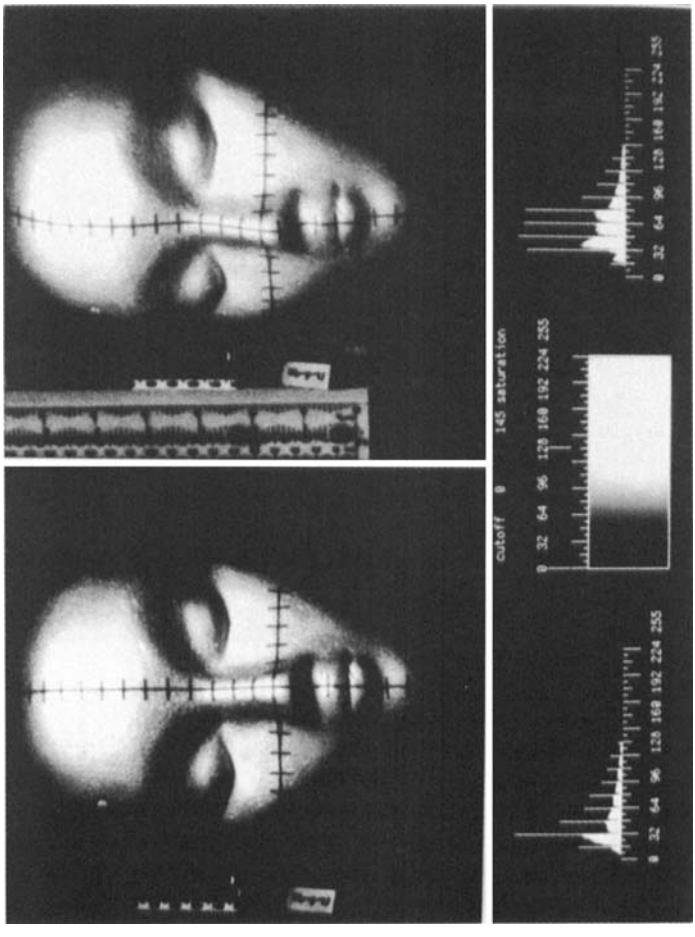

Figure 11. Accuracy assessment object illuminated by diffuse light source.

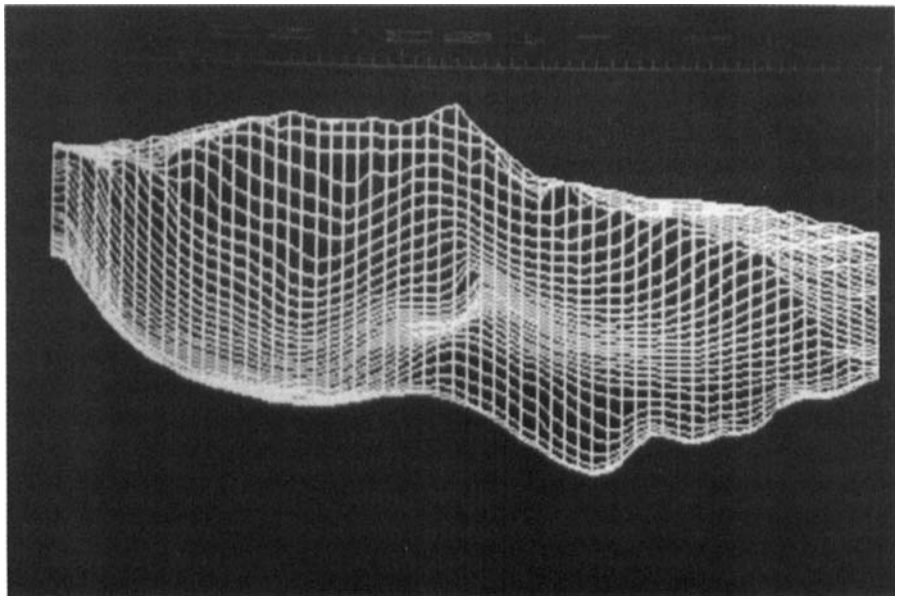

Figure 10. Wireframe representation produced from 3D data measured by the system.

a much more challenging problem than that associated with dimensional assessment of typical mechanical parts.

Automated accuracy assessment has been attempted in the past on an accurately machined cube and cylinder, these being easy to define mathematically for comparison of simulated and measured surface coordinates [22]. The quality of results obtained on a flat or smoothly varying surface, such as these simple objects, gives only an indication of the performance of the system on complex regions of the human face such as the nose or mouth. Comparison in three dimensions (rather than reduction to comparison of lengths) has been used in this study for a small but representative subset of the total surface points measured.

The reference data set had to consist of measurements on a stable object with similar optical and surface characteristics to the human face. A polystyrene model head, marked up with sagittal and coronal lines, together with a series of perpendicular tick marks at regular intervals (as seen in figure 11) formed a suitable reference object. The 3D coordinates of the intersections were measured on a manual electromechanical device with measurement precision of the order of 0·1 mm and defined the global orthogonal coordinate system.

Before use the biostereometric system was calibrated in the usual way and a number of stereo images obtained of the model head (set A) using firstly diffuse illumination and then the boldest speckle pattern originally used in the industrial studies (figure 6). The system was calibrated again and a further set of stereo images (set B) obtained with the less intrusive grid pattern used in the original manual contour measurement work (figure 7). The 3D coordinates of the intersections were then determined in two ways for each data set, using the biostereometric system.

Firstly, the image coordinates of the intersections were manually measured in each image on the workstation. The resulting disparity data were processed to yield 3D coordinates.

Secondly, seed points were measured to initiate the automatic stereo matching of over 5000 data points. Figure 12 shows diagrammatically the relationship between disparity data points and surface data points. The sheet growing algorithm propagates disparity information on a regular grid in the left image. The data points on the object and the disparity data in the right image form a distorted grid due to the combination of the variation in depth across the surface and the effect of perspective. The image coordinate *P left* of the point on the surface *P surface* has position *P right* in the right image. Note that *P surface* does not correspond to any particular visible feature on the surface; choice of this particular element of the surface is a function only of the grid in the left image used as a sampling basis for the sheet growing algorithm. Figure 13 shows the interpolation scheme for measurement of the 3D coordinates of the marker intersections from the automatically generated gridded surface data. The relative position of the left image coordinate to the adjacent grid points is combined with the 3D data at each grid point in a weighting function that determines the 3D position of the tick mark intersection.

The 3D coordinates obtained for the tick mark intersections on the model were in two independent frames of reference due to repositioning of the model and adjustments to the cameras. The optimum translation, rotation and scaling parameters between biostereometric results and the reference coordinates were then determined using a least-squares adjustment to minimize the residual positional error between the pairs of 3D intersections in the global frame of reference. Each data set was further subdivided into measurements made on images with no

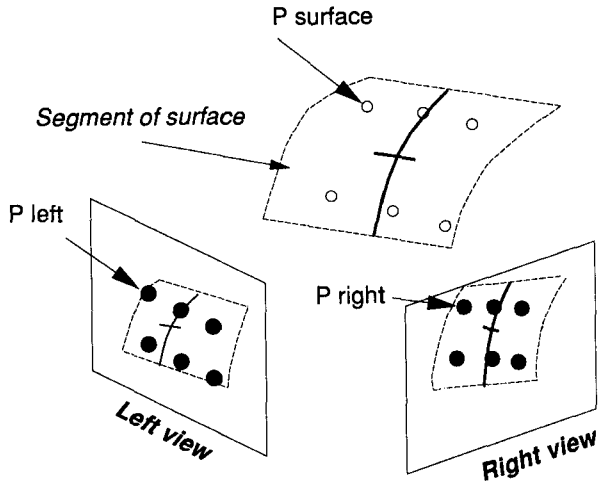

Figure 12. Simplified model of the formation of gridded disparity data using the automatic stereo matching algorithm. Note that the unstructured light pattern has not been shown on the surface.

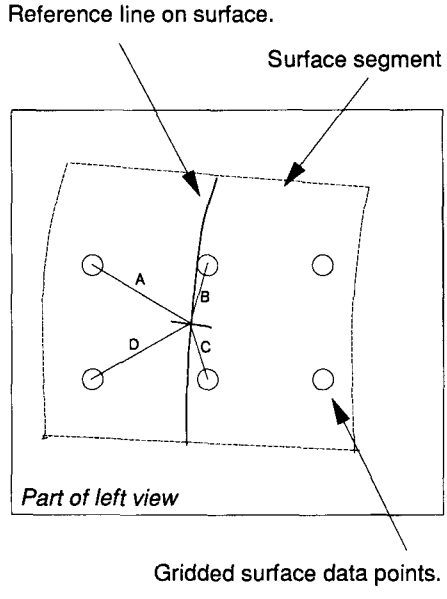

Figure 13. Interpolation of surface is based on the relative distances, measured on the image, of the reference point and the nearest four stereo matched data points (lines marked A, B, C and D).

magnification and ×3 magnification. Manual and automatic results for the transformation parameters are given in table 1.

Determination of the translation and rotation parameters is very consistent, the magnitude of the difference vector at ×3 magnification is only 0·38 mm for the two sets.

Once all points had been aligned with the reference set a small residual error remained. The statistics of this error are summarized in table 2. The minimum residual error vectors are obtained with manual measurement at high magnification (×3). Automatic stereo matching in these cases produces slightly poorer results that are comparable with manual measurements with no image magnification, indicating

Table 1. Mapping parameters for test object consisting of translation and rotation between automatic biostereometric system trials and reference data obtained using high-accuracy manual electromechanical system.

Data description			Translation (mm)			Rotation (degrees)			
Set	Man/auto[a]	Magnification	*Xt*	*Yt*	*Zt*	Omega	Phi	Kappa	Scale
A	Man	×1	−7·45	76·30	121·9	−179·0	17·77	42·00	0·9998
	Auto	×1	−7·54	77·42	121·9	−178·6	17·94	41·80	1·0021
	Man	×3	−7·61	76·84	121·7	−178·8	17·90	41·80	1·0000
	Auto	×3	−7·62	77·30	121·7	−178·8	18·10	42·16	1·0010
B	Man	×1	−10·97	88·92	123·8	−175·4	21·91	40·33	1·0525
	Auto	×1	−8·85	86·55	119·8	−175·0	20·94	41·18	0·9991
	Man	×3	−8·89	86·59	120·0	−175·0	20·86	40·96	0·9997
	Auto	×3	−8·94	86·50	119·7	−175·0	20·98	41·05	0·9974

[a] Man, manual; auto, automatic.

Table 2. Statistics of residual error after remapping of coordinate systems (number of data points: set A, 33; set B, 31).

			Average error vector (mm)			Standard deviation of error vector components σ_{n-1}			Average length of residual error vector (mm)
Set	Man/auto[a]	Magnification	*X*	*Y*	*Z*	*x*	*y*	*z*	
A	Man	×1	0·01	10^{-6}	10^{-6}	0·29	0·48	0·31	0·634
	Auto	×1	0·04	0·04	0·01	0·42	0·45	0·39	0·727
	Man	×3	0·06	−0·01	−0·09	0·11	0·36	0·23	0·462
	Auto	×3	10^{-6}	0·06	10^{-4}	0·45	0·29	0·35	0·623
B	Man	×1	0	10^{-6}	10^{-6}	0·30	0·50	0·33	0·654
	Auto	×1	10^{-6}	10^{-5}	10^{-4}	0·35	0·48	0·33	0·761
	Man	×3	10^{-6}	10^{-6}	10^{-6}	0·30	0·30	0·26	0·492
	Auto	×3	10^{-6}	10^{-6}	10^{-6}	0·41	0·44	0·35	0·682

[a] Man, manual; auto, automatic.

that the grid pattern used in the original manual contour measurement work is not ideally suited for use with the current pair of cameras. A wider range of projected patterns will need evaluation.

6. Discussion

The measurement of facial soft tissue is fundamental to three-dimensional planning of cosmetic surgery procedures, growth studies and objective deformity analysis. The use of high-resolution computer displays offers a very effective means of allowing analysis and further data extraction from the database with a minimum of training and tailoring of systems to the exact requirements of the physician.

Established photogrammetric techniques offer high accuracy but with time-consuming manual analysis. Laser scanning systems can acquire surface data at rates in excess of 700 points per second with measurement accuracy better than 0·5 mm, but these require the patient to remain still for several seconds. Phase analysis of Moiré fringes can utilize high-speed image capture, but in both these techniques fusion of original patient images, surface data and anatomical landmarks can be

difficult. CCD-based biostereometrics offers rapid image capture, which is particularly important in the measurement of young children or patients who are mentally confused or have impaired muscular control, and patient images that retain important landmarks for registration.

The current data-processing bottleneck is the automated stereo matching. The purpose of this study had been to evaluate the measurement performance using an existing computer rather attempt to minimize the processing time. A simple way to reduce the execution time of the sheet growing stereo matching algorithm is to run it on the more powerful workstations now available.

Improvements by a factor of four have been obtained using a Sun SPARCstation™ operating at 12·5 MIPs, yielding a full-face data set of over 5000 data points in under 10 min. If faster data-processing is required a modified version of the algorithm can be executed in parallel. Tests on a PARSYS™ reconfigurable transputer array indicate that the use of 32 T800 25 MHz transputers could reduce processing to under 30 s. The interaction of the sheet growing algorithm and the farming of the processing to the transputer array does, however, introduce further complexity not encountered in the use of serial computing platforms.

Facial analysis falls into three categories: *comparative analysis* in which the surface data are compared directly with previous spatial data sets (monitoring of swelling is an example of this), *composite analysis* involving the use of data acquired by other means (NMR, SPECT, X-ray) and *predictive analysis* which utilizes computer graphics and CAD techniques to evaluate the resulting changes in appearance following treatment. The computer-aided surgical planning system already in use at King's College Hospital is capable of predictive analysis of postoperative soft-tissue *profiles*. Extension to full-face surface shape prediction would dramatically increase the communication of the effects of the planned procedure to the patient. Measurement of surface shape is one input to all these processes, but an equally important element has to be *registration*, either with previous surface information or data describing the underlying bone structure. Stable visible landmarks in the stereo images used in biostereometrics offer a means of reference for registration between data sets obtained using the system. Registration of bone and soft-tissue data and the relationship between changes in bone position and soft-tissue shape present important areas of research.

The quality of stereo image measurement (and hence 3D measurement accuracy) of a point on the surface of the face is to some extent a function of the local rate of change in surface shape.

The stereo correlation patch is chosen to allow a reasonable approximation correspond to a piecewise flat component of the surface, minimizing the inherent averaging effect. Use of higher-resolution imaging technology, and hence a reduction in the spatial pixel size, allows further improvement if necessary. In addition these cameras avoid the use of CCTV video standards and instead allow direct digital sampling of a higher resolution CCD array.

Spatial measurements can be obtained only for regions of the face that appear in both the left and right images. In the current configuration the side of the nose presents a problem in human subjects. This problem could be solved by the use of additional CCD cameras. The current sampling density is uniform in the left (reference) image and, allowing for perspective distortion, approximately uniform over the surface of the face. Good imaging of the central region of the face would

prove important if adaptive sampling algorithms were employed. These would increase the density of surface points measured in regions of the face where rapid changes in shape occur.

The task of high-density, cost-effective, non-contact soft-tissue measurement can now be met by a number of contemporary technologies. There can be little doubt that biometric applications once thought impractical for widespread use on the grounds of speed or cost will be revisited. In addition the application of modern computer-aided design techniques for analysis of 3D data offers considerable potential.

7. Conclusions

This study has evaluated the application of modern imaging technology in the established science of biostereometrics. The measurement accuracy meets the requirements for surgical planning and treatment monitoring. If required, improved accuracy can be achieved through use of larger-format CCD cameras designed for direct interfacing to computer framestores. Image acquisition is rapid, and with suitable choice of unstructured light projection, anatomical landmarks can be retained for registration. Although the automated stereo matching is computationally expensive, modern computing platforms offer a data rate of 8–10 surface points per second; the use of parallel computing techniques can dramatically increase this.

In facial applications, the widespread acceptance of 3D non-contact biometric systems will depend largely on the effectiveness of the composite registration of internal and external data necessary for a valuable analytical and predictive medical system to be produced.

References

1. MacLeod, A. (1986) Medical applications of close range photogrammetry. *Photogrammetric Record*, **12** (68), 155.
2. Moss, J. P., Linney, A. D., Grindrod, S. R., Arridge, S. R., and Clifton, J. S. (1987) Three-dimensional visualization of the face and skull using computerized tomography and laser scanning techniques. *Journal of Orthodontics*, **9**, 247.
3. Miskin, E. A. (1956) The applications of photogrammetric techniques to medical problems. *Photogrammetric Record*, **2**, 92.
4. Burke, P. H. and Beard, L. F. (1967) Stereophotogrammetry of the face. *American Journal of Orthodontics*, **53**, 769.
5. Ruther, H. and Parkyn, N. (1990) Near real-time photogrammetry on a personal computer. *Photogrammetric Record*, **13** (75), 415.
6. Björn, H., Laundqvist, C., and Hjelmström, P. (1954) A photogrammetric method of measuring the volume of facial swellings. *Journal of Dental Research*, **33** (3), 295.
7. Meaney, F. J., and Farrer, L. A. (1986) Clinical anthropometry and medical genetics: a compilation of body measurements in genetic and congenital disorders. *American Journal of Medical Genetics*, **25**, 343.
8. Moss, J. P., Grindrod, S. R., Linney, A. D., Arridge, S. R., and James, D. (1988) A computer system for the interactive planning and prediction of maxillofacial surgery. *American Journal of Dentofacial Orthopedics*, **94**, 469.
9. Burke, P., Banks, P., Beard, L. F., Tee, J., and Hughes, C. (1984) Stereophotographic measurement of change in facial soft tissue morphology following surgery. *British Journal of Oral Surgery*, **21** (4), 237.
10. Burke, P. H. (1980) Serial growth changes of the lips. *British Journal of Orthodontics*, **7**, 17.
11. Saumarez, R. C. (1986) Automated optical measurements of human torso surface movements during breathing. *Journal of Applied Physiology*, **60** (2), 702.
12. Herron, P. H., Cuzzi, J. R., and Richards, T. G. (1970) Stereometric measurement of body and limb volume changes during extended space missions. *Bulletin of the Society for Fr. Photogrammetry*, **40**.
13. Bhatia, S. N., and Sowray, J. H. (1984) A computer-aided design for orthognathic surgery. *British Journal of Oral and Maxillofacial Surgery*, **22**, 237.

14. THOMAS, H. (1989) M.Sc. dissertation, Department of Photogrammetry and Surveying, University College London.
15. BHATIA, S. N., and HARRISON, V. E. (1987) Operational performance of the travelling microscope in the measurement of dental casts. *British Journal of Orthodontics*, **14**, 147.
16. BEYER, H. A. (1987) Some aspects of the geometric calibration of CCD cameras. *Proceedings, ISPRS Intercommission Conference on 'Fast Processing of Photogrammetric Data'*, Interlaken, 2–4 June, pp. 68–81.
17. TSAI, R. Y. (1986) An efficient and accurate camera calibration technique for 3D machine vision. *Proceedings, IEEE Computer Society Conference on Computer Vision and Pattern Recognition*, pp. 364–374.
18. ANTHONY, A. G., DEACON, A. T. and MULLER, J.-P. (1988) A close range vision cell for direct input to CAD systems. *IAPR Workshop on Computer Vision*, October, pp. 12–14.
19. HINTZ, R. J., THOMAS, I. T. and MERCHANT, R. K. (1986) Delineation of craniofacial abnormalities of the fetal alcohol syndrome by close range photogrammetry. *Proceedings, American Society for Photogrammetry and Remote Sensing*, pp. 101–109.
20. OTTO, G. P., and CHAU, T. K. W. (1989) 'Region growing' algorithm for matching of terrain images. *Image and Vision Computing*, **7** (2), 83.
21. GRUEN, A. W. (1985) Adaptive least squares correlation: a powerful image matching technique. *South African Journal of Photogrammetry, Remote Sensing and Cartography*, **14** (3), 175.
22. JACKSON, S. J. (1989) Industrial stereo quality assessment and tuning on the SUN, Part II. *Report Real-time 2.5D Vision Systems*. Alvey/DTI MMI-137.